PHYSICAL REVIEW B **99**, 094506 (2019)

Electrodynamics of granular aluminum from superconductor to insulator: Observation of collective superconducting modes

F. Levy-Bertrand,[1,*] T. Klein,[1] T. Grenet,[1] O. Dupré,[1] A. Benoît,[1] A. Bideaud,[1] O. Bourrion,[2] M. Calvo,[1] A. Catalano,[2] A. Gomez,[3] J. Goupy,[1] L. Grünhaupt,[4] U. v. Luepke,[4] N. Maleeva,[4] F. Valenti,[4] I. M. Pop,[4,†] and A. Monfardini[1,‡]
[1]*Université Grenoble Alpes, CNRS, Grenoble INP, Institut Néel, 38000 Grenoble, France*
[2]*Laboratoire de Physique Subatomique et de Cosmologie, Université Grenoble Alpes, CNRS, 53 rue des Martyrs, 38026 Grenoble Cedex, France*
[3]*Centro de Astrobiología (CSIC-INTA), Ctra. Torrejón-Ajalvir km.4, 28850 Torrejón de Ardoz, Madrid, Spain*
[4]*Physikalisches Institut, Karlsruhe Institute of Technology, 76131 Karlsruhe, Germany*

(Received 22 January 2018; revised manuscript received 25 January 2019; published 8 March 2019)

We report on a detailed study of the optical response and T_c-ρ phase diagram (T_c being the superconducting critical temperature and ρ the normal state resistivity of the film) of granular aluminum, combining transport measurements and a high resolution optical spectroscopy technique. The T_c-ρ phase diagram is discussed as resulting from an interplay between the phase stiffness, the Coulomb repulsion, and the superconducting gap Δ. We provide direct evidence for two different types of well resolved subgap absorptions, at $\omega_1 \simeq \Delta$ and at $\Delta \lesssim \omega_2 \lesssim 2\Delta$ (decreasing with increasing resistivity).

DOI: 10.1103/PhysRevB.99.094506

I. INTRODUCTION

In principle, superconductors are perfect mirrors and no optical absorptions are expected to be observed below twice the superconducting gap 2Δ [1] (for a fully gapped s-wave symmetry). Indeed, amplitude fluctuations of the superconducting order parameter are expected to give rise to a (scalar) mode at 2Δ, decoupled from electromagnetic waves and the dispersive phase fluctuation (Goldstone) mode [2,3] transforms into a nondispersive plasma mode, well above the superconducting gap, in the presence of unscreened long range Coulomb interactions [4,5]. However, an excess of optical absorption below 2Δ has been observed in various disordered superconductors. In NbN and InO this excess has been attributed to the existence of an amplitude (Higgs) mode [6] which could turn into a subgap excitation in the vicinity of a quantum critical point (while approaching a superconductor-to-insulator transition). Alternatively, in granular aluminum, this effect has been discussed as evidence for Goldstone modes [7] turned into a subgap excitation due to the coupling of the linear dispersion with a characteristic finite momentum set in by disorder.

We present here a detailed study of the electrodynamic properties of a series of granular aluminum thin films, combining transport measurements and sub-THz optical spectroscopy. Granular aluminum is formed of superconducting nanometric grains of pure aluminum coupled by Josephson barriers through aluminum oxide, and can be tuned from a superconductor to an insulator by varying the Josephson coupling. The superconducting-insulator transition is reached when the aluminum oxide barriers are too large, preventing a phase coherence to develop throughout all grains [8]. The superconducting critical temperature then presents a dome shape [9–14], whose origin is still debated, with a critical temperature T_c reaching 2–3 K (depending on grain size morphology) at the maximum of the dome, which is significantly higher than the $T_c \sim 1$ K of pure aluminum.

Our optical spectroscopy technique, combining an optical dilution fridge (with a base temperature of $\sim$100 mK) with a Martin-Puplett spectrometer of high resolution (1 GHz) from 0 to 300 GHz enabled us to observe two different types of subgap optical absorptions. We observe first a series of well defined absorption peaks at a frequency ω_1 of the order of Δ and a second larger peak at a frequency ω_2 which decreases progressively from $\sim 2\Delta$ towards $\sim\Delta$ as the superconductor-insulator transition is approached. The onset of those subgap absorptions occurs in the vicinity of the maximum of the superconducting dome, for 100–1000 $\mu\Omega$ cm room temperature resistivity. In the same resistivity range we observed (i) a change from a positive to negative temperature dependence of the normal state resistivity, (ii) an increase of the coupling strength ratio Δ/T_c from $\sim$1.78 to $\sim$2.10, and (iii) we estimate that the phase stiffness J falls below the geometrical Coulomb repulsion energy. Finally, we show that the insulating regime is reached when $\Delta \sim J$.

II. EXPERIMENT

We performed optical spectroscopy and transport measurements on ten samples from low (sample A) to high (sample J) room-temperature resistivity, spanning the phase diagram of granular aluminum from superconductor to insulator. The partial oxygen pressure was increased from samples A to J while e-beam evaporating aluminum at 0.3 nm/s on sapphire substrates held at room temperature. A study of the films

---

[*] florence.levy-bertrand@neel.cnrs.fr
[†] ioan.pop@kit.edu
[‡] alessandro.monfardini@neel.cnrs.fr

TABLE I. Samples studied where ρ is the normal state resistivity, d is the film thickness, T_c is the critical temperature, Δ is the superconducting gap, and L_k is the kinetic inductance.

	ρ ($\mu\Omega$ cm)	d (nm)	T_c (K)	Δ (K)	L_k (pH/sq)
A	40	20	1.90 ± 0.02	3.4 ± 0.3	20
B	80	20	2.04 ± 0.03	3.6 ± 0.1	33
C	160	20	2.17 ± 0.02	3.8 ± 0.1	80
D	220	20	2.17 ± 0.02	3.9 ± 0.1	110
E	900	20	2.08 ± 0.02	4.3 ± 0.3	325
F	1 600	20	2.03 ± 0.06	4.4 ± 0.4	430
G	2 000	20	1.99 ± 0.06	4.3 ± 0.3	535
H	3 000	30	1.91 ± 0.04	3.9 ± 0.1	620
I	11 400	20			
J	20 500	50			

structure prepared in similar conditions allows us to estimate that the grain size is of the order of ~3–4 nm in our films [11]. The films are 20 nm thick except sample H which is 30 nm thick and sample J which is 50 nm thick. On each film, a $3 \times 0.4\,\text{mm}^2$ rectangle has been lithographed in order to perform resistivity measurements. Table I lists the different samples.

The optical spectroscopy technique used here is inspired by millimeter astrophysics observation techniques [15,16]. For each granular aluminum composition, from sample A to H, superconducting microwave resonators were lithographed and cooled down to 100 mK in an optical dilution fridge (those measurements could not be performed in samples I and J for which the resistivity remains finite down to the lowest temperatures). The optical spectroscopy measurements consisted in monitoring the resonators resonance frequencies f while varying the optical incident photon energy. The energy of the incident photon was spanned from 0 to 3 THz with a resolution of ~1 GHz thanks to a Fourier-transform spectrometer with a 300 K black body radiation source. An optical low pass filter in the dilution fridge limits the incident photon range to 300 GHz. Figure 1 presents the resonators design and a schematic view of the experimental setup employed to perform the optical spectroscopy measurements.

The resonance frequency $f = 1/(2\pi\sqrt{LC})$ is of the order of few GHz (from 2 to 6 GHz) and is varied from one resonator to another by varying the capacitor fingers length [see Fig. 1(b)]. The inductance is identical for all the resonators and can be decomposed in a geometric and a kinetic part: $L = L_g + L_k$. The shift of the resonance frequency is due to the change of the kinetic inductance that is inversely proportional to the superfluid density n_s [15,17]:

$$\frac{\delta f}{f} = -\frac{\alpha}{2}\frac{\delta L_k}{L_k} = \frac{\alpha}{2}\frac{\delta n_s}{n_s}, \tag{1}$$

where $\alpha = L_k/(L_k + L_g)$ is the kinetic inductance ratio. The superfluid density may be affected through two different mechanisms by an incident photon $h\nu$. First, when $h\nu > 2\Delta$, the incident photon may break Cooper pairs [15]. Second, for $h\nu < 2\Delta$, superconductors are usually considered as perfect mirrors. One key point of this latter mechanism is the photon absorption. To be absorbed, the energy of an incident photon has to match the energy of a superconducting collective mode.

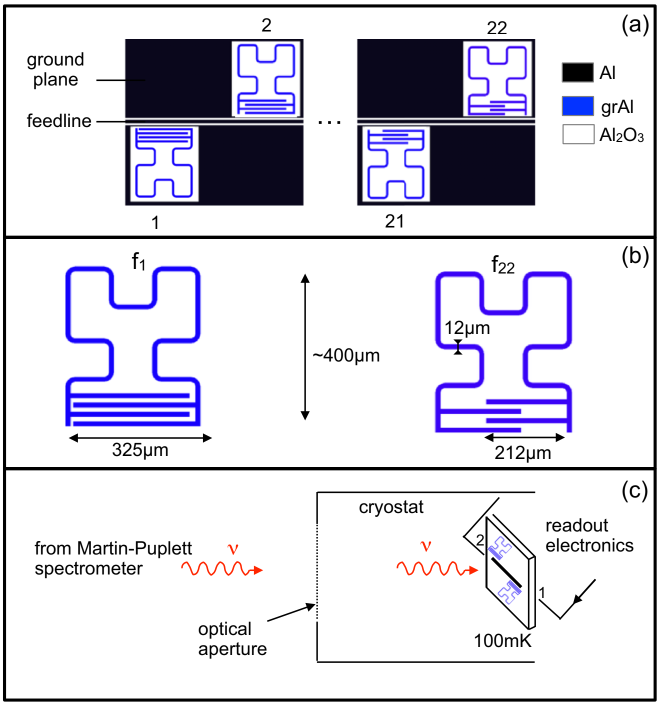

FIG. 1. Resonators design and experimental setup. (a) Sketch of the 22 resonators made out of granular aluminum (grAl in blue) are coupled to the common feed line made out of pure aluminum (Al in black). The feed line and ground plane are in a coplanar waveguide configuration. The dielectric employed is sapphire (Al_2O_3 in white). (b) Detailed design of the first (f_1) and last (f_{22}) resonators. The Hilbert fractal inductor is identical for all the resonators. The four capacitor fingers length are varied from one resonator to another: from the shortest (f_{22}) to the longest (f_1). (c) Experimental setup. Incident photons coming from a Martin-Puplett spectrometer at room temperature illuminates the resonators through the optical apertures of the dilution refrigerator. The variation of the resonance frequencies are measured simultaneously for all the resonators by special readout electronics.

When the photon is absorbed, the superfluid current density J increases, decreasing the superfluid density n_s [18,19], leading to an increase of the kinetic inductance L_k, which can be written as [18–20]

$$L_k(J) = L_k(0)[1 + J^2/J_*^2], \tag{2}$$

where J_* is proportional to the critical current J_c ($J_* = 2/3^{3/2} J_c$ in thin films). J_*^2 sets the incident power scale for which this second mechanism may be observed. This value lowers with the superfluid density (while approaching the superconductor-to-insulator transition for example). Some of us observed this second mechanism in amorphous indium oxide resonators where the collective modes at play were higher-order resonance (surface plasma) modes [21]. For each granular aluminum film from A to H the optical response displayed is an average over all the functional resonators and corresponds to a Fourier transform of the measurements (the individual resonators' responses are displayed in the Appendix). The amplitude of the frequency shift is uncorrected from the incoming source energy distribution and thus is given in arbitrary units.

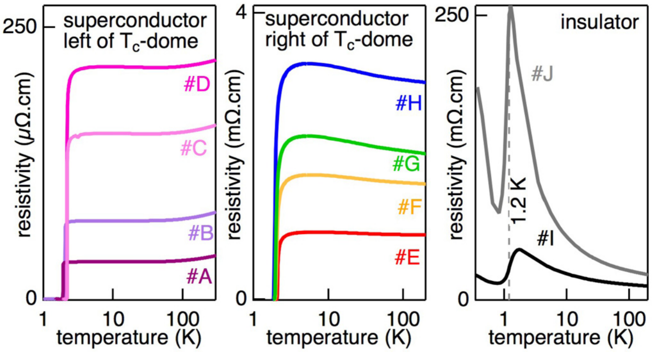

FIG. 2. Superconductor to insulator transition observed through resistivity measurements. Resistivity as a function of temperature for ten different compositions of granular aluminum, from less resistive, sample A, to insulators, samples I and J.

III. RESULTS AND DISCUSSION

A. Transport measurements

As shown in Fig. 2, a superconductor to insulator transition is visible on the resistivity measurements. The room temperature resistivity increases from sample A to sample J. From samples A to D, situated on the left side of the critical superconducting temperature dome, a (mainly) positive slope of the resistivity with temperature is observed and superconductivity develops at low temperature with T_c progressively rising up to ∼2 K (see Fig. 3). As previously reported [11,22–24], a change to a negative slope of the resistivity with temperature is observed in samples E to J (right side of the critical superconducting temperature dome) but superconductivity (null resistance) still develops at low temperature in samples E to H. This change in $d\rho/dT$ may be due either to weak localization effects [25] or to an interplay between electron-phonon coupling and disorder [26–28].

Finally, the temperature dependence of the resistivity in samples I and J can be well described by a $R \propto \exp(T_0/T)^\alpha$ law (with $\alpha \sim 0.25$–0.35) both below and above the dip at 1.2 K, clearly indicating that those films are insulating, at least down to 400 mK. As theoretically foreseen [8] and previously observed [29,30], this dip is a probable reminiscence of local superconductivity in the grains and occurs at the critical temperature of pure aluminum $T_c \sim 1.2$ K (inflection point of the resistive transitions, preliminary resistivity measurements—not presented here—show that the dip disappears for increasing magnetic field, supporting this interpretation). This observation is puzzling as it is often believed that small aluminum grains may have a critical temperature larger than the bulk value [31]. The dip occurring at 1.2 K could hence be the signature of the presence of big clusters of well coupled grains but it may also indicate that the enhanced critical temperature in granular aluminum requires an alternative explanation than shell effects (note that measurements on individual nanometer-scale aluminum particles indicated a constant superconducting gap value, uncorrelated with the radius of the particles [32]).

As shown in Fig. 3, the superconducting transitions are pretty stiff for the samples situated on the left side of the T_c dome, i.e., displaying a (mainly) positive slope of the temperature dependence of the resistivity, and broaden in the samples situated on the right side of the T_c dome (with a negative slope of the temperature dependence of the resistivity). The critical temperatures have then been defined as the inflection point of the resistive transitions (black disks in Fig. 3). The bottom part of the figure displays the critical temperatures versus room temperature resistivity.

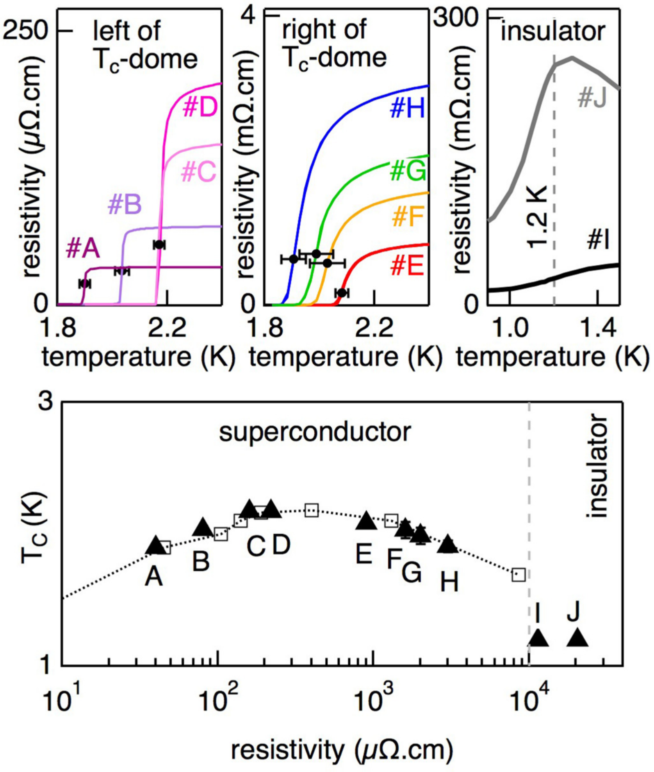

FIG. 3. Critical temperatures determined by resistivity measurements. *Top panel:* Zoom on the superconducting transition of the resistivity measurements as a function of temperature. Critical temperatures, black disks, correspond to the inflection point of the resistive transitions. Error bars are the temperature intervals between zero resistivity and the inflection point. *Bottom panel:* Critical temperatures versus room temperature resistivity. The dashed line connects the squares corresponding to critical temperatures of samples deposited by some of us on a different substrate (silicon) using a different e-beam deposition device.

B. Phase diagram

Figure 4 displays the phase diagram of granular aluminum, presenting the evolution with resistivity of the different energies at play. Following Ref. [14], Fig. 4(a) displays the critical temperature, the superconducting gap (deduced from our optical measurements, see below), the phase stiffness, and the Coulomb repulsion energy. The phase stiffness of the superconducting condensate determines the phase coherence of the condensate and corresponds to the Josephson energy in the case of a network of Josephson junctions. At zero temperature, J can first be evaluated through $J_\Delta = \frac{\hbar}{4e^2}\frac{\pi\Delta}{R_{\rm sq}}$ [7,8,12,14] where $R_{\rm sq}$ is the thin film surface resistance per square (labeled J_Δ in Fig. 4). J is also related to the

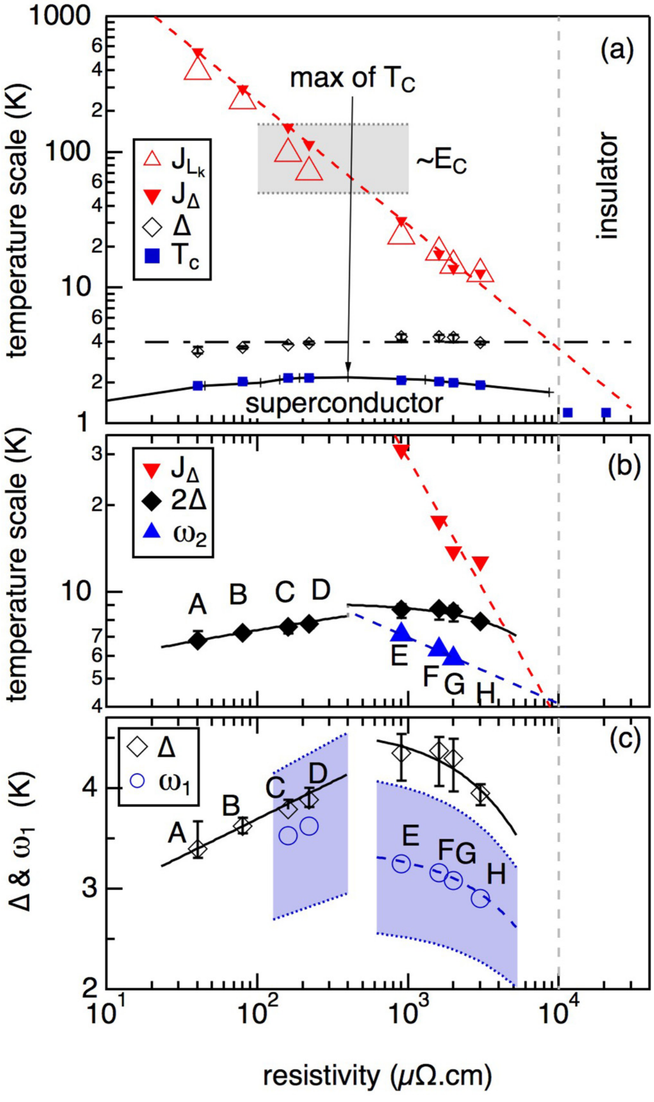

FIG. 4. Phase diagram of granular aluminum: Evolution of energies at play for increasing resistivity. (a) Critical temperature T_c, superconducting gap Δ, phase stiffness J_Δ and J_{L_s}, and Coulomb repulsion energy E_c. The continuous black line with crosses corresponds to a critical temperature of samples deposited by some of us on a different substrate (silicon). Dashed lines are linear guides to the eyes. (b) Evolution of J_Δ, 2Δ, and the subgap optical absorption ω_2. The ω_2 points correspond to the energy of the ω_2 features maxima. The ω_2 dashed line slope is four times smaller than that of J_Δ. (c) Evolution of Δ and ω_1. The ω_1 points correspond to the mid-position of the ω_1 distribution. The energy distribution of ω_1 is depicted by the shade area. The Δ continuous lines are a guide to the eyes. The ω_1 dashed line is the Δ continuous line divided by 1.35.

kinetic inductance of the superconducting resonators L_k though $J_{L_k} = \frac{\hbar^2}{4e^2 L_k}$ [33]. By comparing their resonance frequencies $f \sim (L_k C)^{-1/2}$ to frequencies obtained by radiofrequency electromagnetic simulations, we determined L_k [21] and thus the phase stiffness labeled J_{L_k}. Those two J values agree with each other very well. The measured data show that superconductivity is suppressed at the superconducting-insulating transition, when the phase stiffness becomes smaller than the superconducting gap.

The Coulomb repulsion energy E_c, i.e., the bare geometrical charging energy, which is the energy cost to transfer an electron from grain to grain, increases with the resistivity [12]. This charging energy can be estimated for a resistivity corresponding to grains just decoupled through one unit cell of the aluminum oxide barrier by [12] $E_c = \frac{e^2}{4\pi\epsilon_0\epsilon_r d}\frac{s}{s+d/2}$, where $\epsilon_r \sim 8.5$ is the relative dielectric constant of aluminum oxide, $s \sim 0.5$ nm correspond to one atomic layer of the insulating barrier, and d is the grain size. Taking $d \sim 3$–6 nm for one to two merging grains [11], one obtains $E_c \sim 100 \pm 50$ K, which is close to the phase stiffness J at the dome maximum.

Granular aluminum films may be described as disordered arrays of Josephson junctions connecting the grains. The phase diagram of granular aluminum can be interpreted as resulting from an interplay between the different energy scales that are the phase stiffness, the Coulomb repulsion, and the superconducting gap [34]. In the metallic regime, for room temperature resistivity $\rho \lesssim 100\ \mu\Omega$ cm, when superconductivity establishes, all electrons condensate and form one wave function with a unique phase. The phase is *rigid* with a phase stiffness J that is orders of magnitude higher than both the Coulomb repulsion energy E_c and the superconducting gap Δ [see Fig. 4(a)]. In the vicinity of the superconducting dome maximum, for $100 \lesssim \rho \lesssim 1000\ \mu\Omega$ cm, the phase stiffness falls below the Coulomb repulsion energy. Note that the Coulomb repulsion energy E_c is not a relevant energy on a microscopic scale as electron tunneling between the grains leads to a renormalization of E_c down to a smaller effective Coulomb energy [34,35] $\tilde{E}_c \sim \Delta^2/J$. However, experimentally $J < E_c$ seems to coincide with the onset of subgap absorptions, a change from a positive to negative temperature dependence of the normal state resistivity, and an increase of the coupling strength ratio Δ/T_c from ~1.78 to ~2.10. In line with Ref. [36] we suggest that for $\tilde{E}_c < J < E_c$ phase fluctuations develop leading to a decrease of T_c. Eventually, when $J < \tilde{E}_c$, Coulomb blockade localizes the Cooper pairs within the grains, turning the system into an insulator [8,34]. The superconductor-insulator transition is theoretically expected to be reached for $J/\tilde{E}_c \sim 1$, i.e., for $J \sim \Delta$, which corresponds to a surface resistance per square equal to the quantum of resistance $h/(2e)^2 \sim 6.4$ kΩ. Indeed, the sheet resistance of the first insulating sample is 5.7 kΩ.

C. Optical response and subgap optical absorptions

In Fig. 5 we show the optical response of superconducting granular aluminum films. Twice the superconducting gap value 2Δ is directly determined from the abrupt increases of the frequency shift as the photon energy $h\nu$ reaches 2Δ (pair breaking). Figure 6 displays the evolution of the superconducting gap and gap over critical temperature ratio as a function of the room-temperature resistivity. The top panel shows that there is a modification of the superconducting coupling parameter Δ/T_c which increases from ~1.78 to ~2.10. The direct comparison of the optical response of sample D ($T_c = 2.17$ K, left side of the T_c dome) to that of sample E ($T_c = 2.08$ K, right side of the T_c dome) underlines that although their critical temperature are almost identical their gap are different (see Fig. 5). Note that the Δ/T_c ratio of sample H, $T_c = 1.91$ K, is clearly larger than ~1.78 including the error

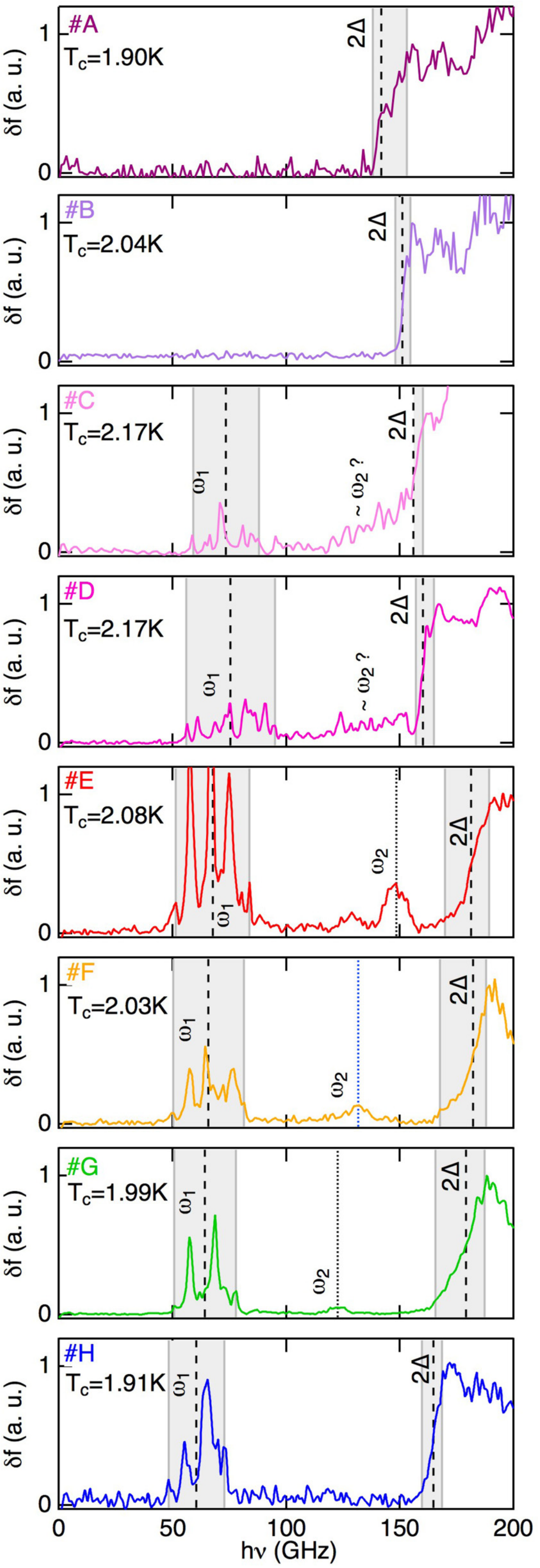

FIG. 5. Optical spectroscopy responses of superconducting granular aluminum films. For increasing resistivity from sample A to H, frequency shift at ∼100 mK as a function of the incident photon energy $h\nu$. The dash line indicates the mid-height position of the 2Δ threshold, the shaded area corresponds to the 10%–90% height area but for sample C due to an excess of optical absorption just below twice the superconducting gap. Below 2Δ two different types of subgap absorptions are observed at ω_1 and at ω_2.

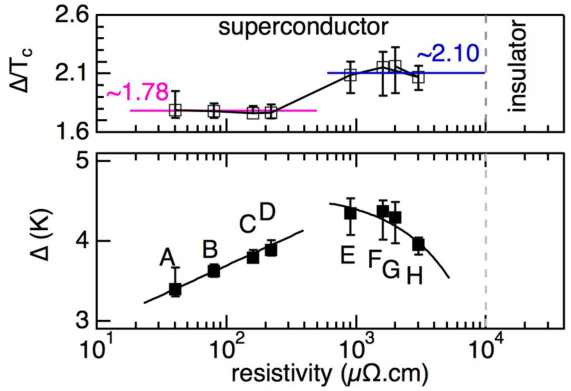

FIG. 6. Evolution with resistivity of the superconducting gap and of the ratio gap over critical temperature. *Bottom panel:* Superconducting gaps Δ measured at ∼100 mK as a function of room temperature resistivity. The error bars correspond to the 10%–90% threshold in the optical response at 2Δ. Continuous black lines are guides to the eyes. *Top panel:* Coupling strength Δ/T_c as a function of room temperature resistivity. Error bars include the error bars coming from T_c (interval from inflection point to zero resistance) and the error bars coming from Δ. Lines are guides to the eyes.

bars. The lines of the bottom panel intend to underline the change of the gap value.

Below 2Δ the superfluid response evolves from a featureless response for samples A and B to a response with strong subgap features for samples E to H. Samples C and D show an intermediate response. Our results are consistent with the excess of optical absorption observed previously below twice the superconducting gap in granular aluminum [7] (and other disordered superconductors [6]). This excess of optical absorption as been interpreted as a Goldstone mode [7] of the superconducting order parameter. As we do show here that those subgap absorptions onset for $J \sim E_c$ and strengthen for $J < E_c$, we confirm that they are probably related to phase fluctuations of the superconducting order parameter.

However, it is important to note that—thanks to a higher energy resolution of our spectrometer and lower working temperature—we can resolve the existence of *two* different types of features, occurring at ω_1 and ω_2 (see Fig. 5). Both the energy position and the shape of those absorption peaks are clearly different. As shown in Fig. 4(c), ω_1 remains on the order of Δ (slightly lower) in all measured samples. This ω_1 feature is rather an assembly of more-or-less distinguishable sharp features spread over a few tens of GHz (the ω_1 dashed line indicates the mid-position of the features, and the distribution is underlined by the shaded area). In Ref. [37] this absorption has been attributed to a two-dimensional plasma phase mode. In two-dimensional superconducting films plasma oscillations are expected to occur for discrete momentum values $k_n = n \times 2\pi/L$ and energy ω_n where n is an integer and L is the length of the thin film/resonator (predicted [38,39] and observed [40]). Those surface plasma modes correspond to the higher order resonance modes of a superconducting resonator and saturate at the two-dimensional plasma frequency where the number of resonances then diverges [37]. In Ref. [37] an analytical plasma dispersion established from a network of Josephson junction model estimates a plasma frequency of 68 GHz from the $n = 1$ and $n = 3$ resonances mode measured on a granular aluminum film with $\rho = 4000\ \mu\Omega\,\text{cm}$, in very good agreement with our observation. However, note that the multiple peak structure of ω_1 remains unexplained within this scenario.

On the other hand, the ω_2 feature is a broad response, the maximum of which is indicated by a dashed line in Fig. 5. This feature is only clearly distinguishable in three samples: E, F, and G (the excess of optical response just below 2Δ in samples C and D may be attributed to this ω_2 feature), and clearly decreases from $\sim 2\Delta$ down to almost Δ as the sample resistivity increases, tending towards J at the superconductor-to-insulator transition [see Fig. 4(b)]. The origin of this feature remains to be explained.

IV. CONCLUSION

In conclusion, we explored the superconducting critical temperature dome shape of granular aluminum by combined state-of-the art optical spectroscopy and resistivity measurements. In the vicinity of the dome maximum, we evidenced a superconducting coupling modification from $\Delta/T_c \sim 1.78$ to $\Delta/T_c \sim 2.10$. Within the same region we observe the occurrence of subgap features in the optical response, the change from a positive to negative temperature slope of the resistivity, and we estimate that the phase stiffness falls below the Coulomb energy. We evidenced two types of subgap excitations below twice the superconducting gap 2Δ and studied their evolution with resistivity.

ACKNOWLEDGMENTS

We are in debt to Lara Benfatto, Régis Mélin, Benoît Douçot, and Olivier Buisson for discussions on the superconducting collective modes. We are very grateful to Pierre Lachkar for his help during the resistivity measurements on the Physical Property Measurement System. We acknowledge the contributions of the Cryogenics and Electronics groups at Institut Néel and LPSC. This work is supported by the French National Research Agency through Grant No. ANR-16-CE30-0019 ELODIS2 and by the LabEx FOCUS through Grant No. ANR-11-LABX-0013. F.L-B. acknowledges financial support from the CNRS through a grant *Défi Instrumentation aux limites 2018*. L.G., U.v.L., N.M., F.V., and I.M.P. acknowledge funding from the Alexander von Humboldt foundation in the framework of a Sofja Kovalevskaja award endowed by the German Federal Ministry of Education and Research. A.G. acknowledges the financial support from Project ESP2015-65597-C4-1-R.

APPENDIX

In Fig. 7 we show, for each granular aluminum film from A to H, the average optical response and the optical response of each functional resonator. The 2Δ threshold and the ω_2 absorption are, within the noise, identical for every functional resonator of a given film. The ω_1 features are different from resonator to resonator. An optical low pass filter in the dilution fridge limits the incident photon range to 300 GHz.

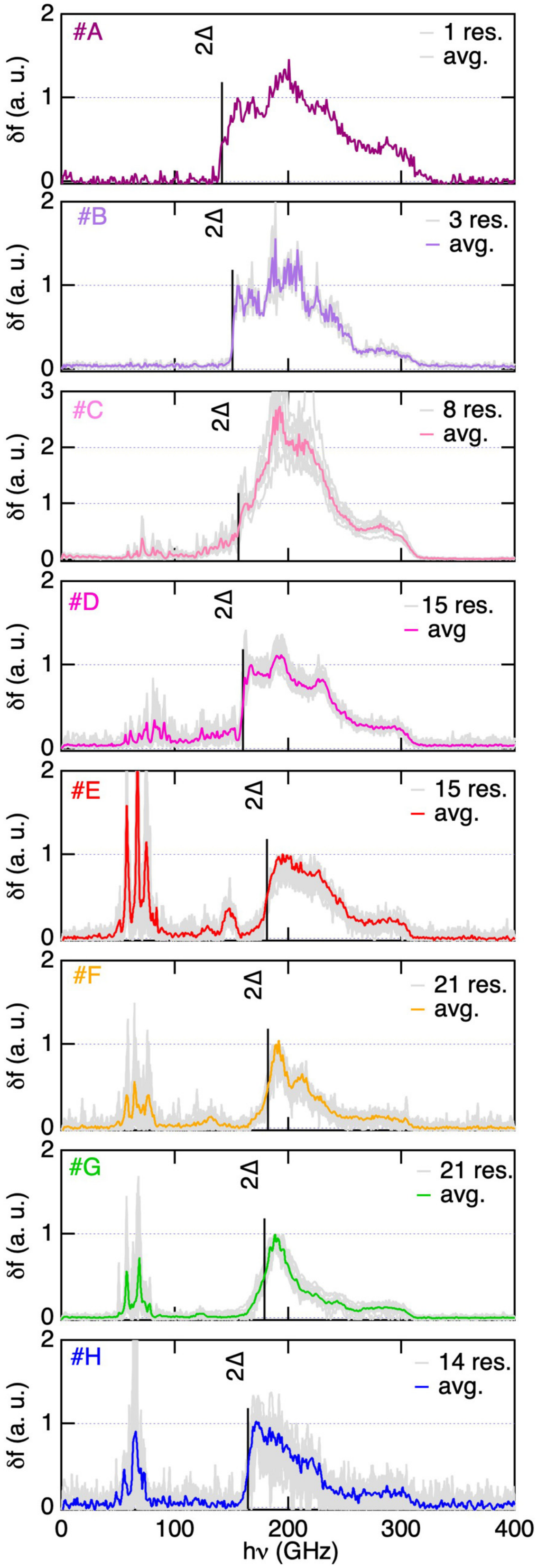

FIG. 7. Optical spectroscopy responses of superconducting granular aluminum films. For increasing resistivity from sample A to H, the average (avg.) and the individual resonator (res.) frequency shift at ~100 mK as a function of the incident photon energy $h\nu$. The line indicates the mid-height position of the 2Δ threshold.

[1] C. M. Varma, J. Low Temp. Phys. **126**, 901 (2002).
[2] Y. Nambu, Phys. Rev. Lett. **4**, 380 (1960).
[3] J. Goldstone, Nuovo Cimento **19**, 154 (1961).
[4] P. W. Anderson, Phys. Rev. **112**, 1900 (1958).
[5] P. W. Anderson, Phys. Rev. **130**, 439 (1963).
[6] D. Sherman, U. S. Pracht, B. Gorshunov, S. Poran, J. Jesudasan, M. Chand, P. Raychaudhuri, M. Swanson, N. Trivedi, A. Auerbach, M. Scheffler, A. Frydman, and M. Dressel, Nat. Phys. **11**, 188 (2015).
[7] U. S. Pracht, T. Cea, N. Bachar, G. Deutscher, E. Farber, M. Dressel, M. Scheffler, C. Castellani, A. M. Garcia-Garcia, and L. Benfatto, Phys. Rev. B **96**, 094514 (2017).
[8] K. B. Efetov, Sov. Phys. JETP **51**, 1015 (1980).
[9] B. Abeles, R. W. Cohen, and G. W. Cullen, Phys. Rev. Lett. **17**, 632 (1966).
[10] R. W. Cohen and B. Abeles, Phys. Rev. **168**, 444 (1968).
[11] G. Deutscher, H. Fenichel, M. Gershenson, E. Grünbaum, and Z. Ovadyahu, J. Low Temp. Phys. **10**, 231 (1973).
[12] N. Bachar, Ph.D. thesis, Tel-Aviv University, Tel-Aviv, Israel, 2014.
[13] N. Bachar, S. Lerer, A. Levy, S. Hacohen-Gourgy, B. Almog, H. Saadaoui, Z. Salman, E. Morenzoni, and G. Deutscher, Phys. Rev. B **91**, 041123(R) (2015).
[14] U. S. Pracht, N. Bachar, L. Benfatto, G. Deutscher, E. Farber, M. Dressel, and M. Scheffler, Phys. Rev. B **93**, 100503(R) (2016).
[15] P. K. Day, H. G. LeDuc, B. A. Mazin, A. Vayonakis, and J. Zmuidzinas, Nature (London) **425**, 817 (2003).
[16] M. Calvo, A. Benoît, A. Catalano, J. Goupy, A. Monfardini, N. Ponthieu, E. Barria, G. Bres, M. Grollier, G. Garde, J.-P. Leggeri, G. Pont, S. Triqueneaux, R. Adam, O. Bourrion, J.-F. Macías-Pérez, M. Rebolo, A. Ritacco, J.-P. Scordilis, D. Tourres, A. Adane, G. Coiffard, S. Leclercq, F.-X. Désert, S. Doyle, P. Mauskopf, C. Tucker, P. Ade, P. André, A. Beelen, B. Belier, A. Bideaud, N. Billot, B. Comis, A. DõAddabbo, C. Kramer, J. Martino, F. Mayet, F. Pajot, E. Pascale, L. Perotto, V. Revéret, L. Rodriguez, G. Savini, K. Schuster, A. Sievers, and R. Zylka, J. Low Temp. Phys. **184**, 816 (2016).
[17] P. Diener, H. Schellevis, and J. J. A. Baselmans, Appl. Phys. Lett. **101**, 252601 (2012).
[18] P. G. De Gennes, *Superconductivity of Metals and Alloys* (Westview, Boulder, CO, 1999), Chap 6.5.
[19] M. Tinkham, *Introduction to Superconductivity* (McGraw-Hill, New York, 1996), Chap. 4.4.
[20] L. J. Swenson *et al.*, J. Appl. Phys. **113**, 104501 (2013).
[21] O. Dupré, A. Benoît, M. Calvo, A. Catalano, J. Goupy, C. Hoarau, T. Klein, K. Le Calvez, B. Sacépé, A. Monfardini, and F. Levy-Bertrand, Supercond. Sci. Technol. **30**, 045007 (2017).
[22] N. Bachar, S. Lerer, S. Hacohen-Gourgy, B. Almog, and G. Deutscher, Phys. Rev. B **87**, 214512 (2013).
[23] K. C. Mui, P. Lindenfeld, and W. L. McLean, Phys. Rev. B **30**, 2951(R) (1984).
[24] M. Kunchur, P. Lindenfeld, W. L. McLean, and J. S. Brooks, Phys. Rev. Lett. **59**, 1232 (1987).
[25] B. L. Altshuler and A. G. Aronov, in *Electron-Electron Interaction in Disordered Conductors*, edited by A. L. Efros and M. Pollak (Elsevier, Amsterdam, 1985).
[26] Y. Imry, Phys. Rev. Lett. **44**, 469 (1980).
[27] M. Jonson and S. M. Girvin, Phys. Rev. Lett. **43**, 1447 (1979).
[28] D. Di Sante, S. Fratini, V. Dobrosavljević, and S. Ciuchi, Phys. Rev. Lett. **118**, 036602 (2017).
[29] H. M. Jaeger, D. B. Haviland, B. G. Orr, and A. M. Goldman, Phys. Rev. B **40**, 182 (1989).
[30] W. Wu and P. W. Adams, Phys. Rev. B **50**, 13065(R) (1994).
[31] J. A. A. J. Perenboom, P. Wyder, and F. Meier, Phys. Rep. **78**, 173 (1981).
[32] C. T. Black, D. C. Ralph, and M. Tinkham, Phys. Rev. Lett. **76**, 688 (1996).
[33] H. Rotzinger, S. T. Skacel, M. Pfirrmann, J. N. Voss, J. Münzberg, S. Probst, P. Bushev, M. P. Weides, A. V. Ustinov, and J. E. Mooij, Supercond. Sci. Technol. **30**, 025002 (2017).
[34] I. S. Beloborodov, A. V. Lopatin, V. M. Vinokur, and K. B. Efetov, Rev. Mod. Phys. **79**, 469 (2007).
[35] A. I. Larkin and Yu. N. Ovchinnikov, Phys. Rev. B **28**, 6281 (1983).
[36] V. J. Emery and S. A. Kivelson, Nature (London) **374**, 434 (1995).
[37] N. Maleeva, L. Grünhaupt, T. Klein, F. Levy-Bertrand, O. Dupre, M. Calvo, F. Valenti, P. Winkel, F. Friedrich, W. Wernsdorfer, A. V. Ustinov, H. Rotzinger, A. Monfardini, M. V. Fistul, and I. M. Pop, Nat. Commun. **9**, 3889 (2018).
[38] T. Mishonov and A. Groshev, Phys. Rev. Lett. **64**, 2199 (1990).
[39] B. Mirhashem and R. Ferrell, Physica C **161**, 354 (1989).
[40] O. Buisson, P. Xavier, and J. Richard, Phys. Rev. Lett. **73**, 3153 (1994); **74**, 1493(E) (1995).